Asymptotic bifurcation solutions for compressions of a clamped nonlinearly elastic rectangle Transition region and barrelling to a corner-like profile

Dai, Hui-Hui; Wang, Fan-Fan

Published in:
SIAM Journal on Applied Mathematics

Published: 01/01/2010

Document Version:
Final Published version, also known as Publisher's PDF, Publisher's Final version or Version of Record

Published version (DOI):
10.1137/090754625

Publication details:
Dai, H.-H., & Wang, F.-F. (2010). Asymptotic bifurcation solutions for compressions of a clamped nonlinearly elastic rectangle: Transition region and barrelling to a corner-like profile. *SIAM Journal on Applied Mathematics*, *70*(7), 2673-2692. https://doi.org/10.1137/090754625

SIAM J. APPL. MATH.
Vol. 70, No. 7, pp. 2673–2692

ASYMPTOTIC BIFURCATION SOLUTIONS FOR COMPRESSIONS OF A CLAMPED NONLINEARLY ELASTIC RECTANGLE: TRANSITION REGION AND BARRELLING TO A CORNER-LIKE PROFILE*

HUI-HUI DAI† AND FAN-FAN WANG‡

Abstract. In the two experiments by Beatty and his coauthors on the compressions of elastic rectangles/bars, it was found that there is a transition region of the aspect ratio which separates buckling from barrelling. Friction, which prevents the lateral movement of the end cross section, might be the cause. Here, we study the compressions with clamped end conditions. One of the purposes is to show, with this setting in which the lateral movement of the end cross section is limited, that there is indeed such a transition region. By using combined series-asymptotic expansions, we derive two decoupled nonlinear ordinary differential equations (ODEs). By phase plane analysis, the leading-order axial strain can be obtained from one of the ODEs. Then an eigenvalue problem can be formulated from another ODE, which is solved by the WKB (Wentzel–Kramers–Brillouin) method. It is found that when the aspect ratio is relatively large there is only a bifurcation to the barrelling which leads to a corner-like profile on the lateral boundaries of the rectangle. When the aspect ratio is relatively small there are only bifurcation points which lead to the buckled profiles. A lower bound of the aspect ratio for barrelling and a different upper bound for buckling are found, which implies the existence of the above-mentioned transition region. Another finding is that, after the barrelling, no further bifurcation to buckling can occur. The critical buckling loads obtained from our asymptotic solutions are also compared with those obtained from the Euler buckling formula.

Key words. nonlinear elasticity, bifurcation, corner-like profile, barrelling, buckling

AMS subject classifications. 74G10, 74G60, 35B32, 34B16

DOI. 10.1137/090754625

1. Introduction.

Two kinds of instabilities, buckling and barrelling, may occur when a two-dimensional nonlinearly elastic rectangle is compressed uniaxially. The classical Euler buckling formula may be used to predict the onset of buckling of a rod. However, the Bernoulli–Euler beam theory does not take into account the effect of transverse shear strain. In this paper, we consider both buckling and barrelling instabilities and present some new analytical postbuckling and postbarrelling results for both thin and moderately thick two-dimensional rectangles with clamped boundary conditions.

Theoretical analysis of this type of compression problems with lubricated boundary conditions has been carried out by many authors; see [1, 2, 3, 4] and their listed references. In these papers, barrelling or buckling instabilities of a rectangle, square column, or circular cylinder were studied. Besides the theoretical analysis in [1, 2, 3, 4], lubricated boundary conditions at two ends were also used in two recent papers [5, 6] concerning buckling and barrelling. In [5], Goriely, Vandiver, and Destrade studied the compression of a three-dimensional incompressible cylindrical tube under axial

*Received by the editors April 1, 2009; accepted for publication (in revised form) May 7, 2010; published electronically July 29, 2010.

http://www.siam.org/journals/siap/70-7/75462.html

†Department of Mathematics and Liu Bie Ju Center for Mathematical Sciences, City University of Hong Kong, 83 Tat Chee Avenue, Kowloon Tong, Hong Kong (mahhdai@cityu.edu.hk). The research of this author was supported by two grants from the Research Grants Council of the HKSAR (Projects CityU 100807 and CityU 101009).

‡Department of Mathematics, City University of Hong Kong, 83 Tat Chee Avenue, Kowloon Tong, Hong Kong (fanfwang@cityu.edu.hk).

load. In [6], Simpson and Spector proved that a rectangular elastic rod will buckle under quasi-static compression at two frictionless ends. Another proof of the existence of a nontrivial bifurcated branch in finite elasticity was given by Healey and Montes-Pizarro [7], and lubricated boundary conditions were also used.

However, in practice and experiments, it is very difficult to realize such lubricated boundary conditions, especially when the external force becomes large. Not so many experimental works on both buckling and barrelling have been carried out. Two well-known experimental works were done by Beatty and Hook [8] and Beatty and Dadras [9]. In [8], circular rubber bars with different aspect ratios ρ (ratio of diameter to length of the cylinder) were compressed at two lubricated ends. It was found that when $\rho < \rho_1 = 0.216$, only buckling could occur, while when $\rho > \rho_2 = 0.228$, only barrelling could occur. There was a "transition region in which the nature of the strut behavior becomes increasingly ambiguous" (see [8, p. 630]). The authors believed that there should be a limiting aspect ratio value in this transition region which separates instability by barrelling from buckling, and this value was estimated to be 0.222 graphically. In another experimental work (Beatty and Dadras [9]), besides circular cylindrical elastomer bars, rectangular bars and thick-walled tubular columns were also compressed at two lubricated ends. In each case a similar "transition region" was found, and similar results were concluded. In [10, 11], Dai and Wang studied the barrelling instability in a circular cylinder leading to a corner-like profile. In this paper, we focus on the transition region observed in the experiments of [8, 9] involving both the barrelling instability and the buckling instability. The existence of the transition region appears to be an interesting problem which has not been solved theoretically, analytically, or numerically. We intend to show the existence of the transition region by explicitly finding an upper bound for buckling and a lower bound for barrelling when a clamped rectangle is compressed at two ends. Also, an important finding is that, after the barrelling, no further bifurcation to the buckling will occur if the external load is increased.

The experimental results of [8, 9] are in good qualitative agreement with the theoretical analysis of Beatty [12]. It should be noted that friction was present at two flat ends, although they were lubricated in experiments. It was also remarked by Beatty and Hook in [8] that "In spite of lubrication, the material consistently tended to adhere to the end plates of the test machine" (see [8, p. 628]), and "We are unable to assess in any case the extent to which end effects may have influenced our measurements" (see [8, p. 630]). So far there is little literature on either experimental results or theoretical analysis of compressions of bars when friction is taken into account. Also the effect of friction on instabilities of bars is not known.

Due to mathematical difficulties in the description of friction, in this paper we analyze the effect of clamped boundary conditions on instabilities. A key feature shared by a clamped constraint and friction is that they both limit the lateral movement of the end cross section. We aim to reveal, with such a constraint, that there indeed exists a transition region as observed in experiments. As far as we know, it seems that no other work has considered such two- or three-dimensional clamped boundary conditions in stability and instability analysis within the framework of nonlinear elasticity. The clamped boundary condition used by others before is mainly a one-dimensional condition which includes only zero lateral displacement and zero slope at the end. Here, by using the combined series-asymptotic expansions, we can obtain asymptotically approximate boundary conditions for a clamped end in the two-dimensional setting.

Another motivation is related to the Euler buckling formula which gives the criti-

cal compressive force when a rod begins to buckle under compression. This formula is based on the Bernoulli–Euler constitutive equation. Here we derive new model equations for the critical stress values where the axial strain is emphasized. Numerical results show that we can obtain an improvement of the first critical stress value.

The structure of this paper is as follows. In section 2, we present the field equations and the traction-free boundary conditions. Due to the difficulty of nonlinearity, we assume that the aspect ratio is small; i.e., we are considering a thin or moderately thick rectangle. Then, in section 3, after nondimensionalization of the field equations and the traction-free boundary conditions, we can identify two small parameters and one small variable. By using the combined series-asymptotic expansions, two decoupled nonlinear ordinary differential equations (ODEs) are obtained. One governs the leading order of the axial strain, which can be written as a singular ODE system. Another governs both the axial strain and the shear strain. These two equations can also be obtained by the variational principle, as shown in section 4. In section 5, by using the combined series-asymptotic expansions, the clamped boundary conditions amount to a set of asymptotically approximate boundary conditions, which are used to determine the axial strain and the shear strain. In section 6, we carry out some bifurcation analysis. By phase plane analysis, the solution of the axial strain can be obtained for the clamped boundary conditions. An asymptotic solution for the shear strain can be obtained through the WKB (Wentzel–Kramers–Brillouin) method. Then the condition for determining the buckling critical stress value is obtained. For some chosen material constants, numerical calculations show that when the aspect ratio is relatively large (within our assumption of a small aspect ratio), there will be no buckling mode. However, there is a bifurcation to a corner-like profile which is a barrelling instability. In terms of a nonsmoothness-like profile, this corner-like profile is related to the Willis instability, which is an interesting phenomenon observed in an experiment done by Willis in [13] (for the description of this instability, see [14]). In [10, 11], Dai and Wang did some analysis and pointed out that this kind of instability could be caused by the coupling effect of material nonlinearity and geometry size. When the aspect ratio is relatively small, only buckling modes can be found. Also, the thinner the rectangle, the more buckling modes are obtained. One important difference between our buckling and previous works is that our buckling is not a special kind of buckling, while buckling considered in some of the previous works such as [3, 4] is an Euler-type buckling, which is very special. A major finding based on the analytical results is that with clamped boundary conditions there is indeed a transition region such that when the aspect ratio is larger than a critical value the barrelling instability occurs, and when it is smaller than another critical value the buckling instability occurs. This reveals the existence of a transition region, which is in agreement with the experimental results of Beatty and Hook [8] and Beatty and Dadras [9]. In section 7, we make our conclusions.

2. Field equations. We study the compressions of a two-dimensional rectangle with two clamped ends, as illustrated in Figure 2.1. This problem can be regarded as a plane strain problem of a cross section of a three-dimensional block with an infinite length in one direction. It is supposed that the block is composed of a compressible hyperelastic material. Let the length of the rectangle be l and the thickness be $2a$, and let (X, Y) and (x, y) denote the Cartesian coordinates of a material point in the reference and current configurations, respectively. The axial and lateral displacements are denoted by

$$U(X,Y) = x - X, \qquad V(X,Y) = y - Y, \tag{2.1}$$

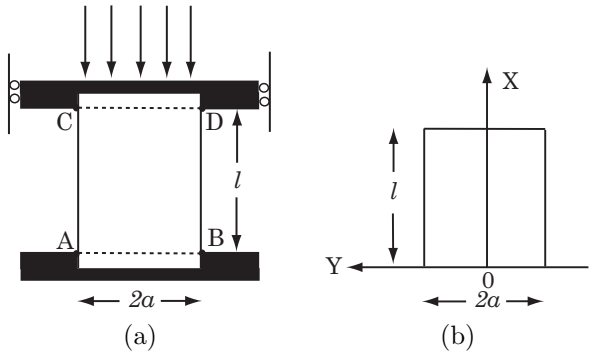

FIG. 2.1. (a) *Geometry of a rectangle with two thin parts clamped at two ends.* (b) *Cartesian coordinates for the object of study.*

respectively. Then the deformation gradient tensor $\mathbf{F}$ is given by

$$\mathbf{F} = (U_X + 1)\mathbf{e}_x \otimes \mathbf{E}_X + U_Y \mathbf{e}_x \otimes \mathbf{E}_Y + V_X \mathbf{e}_y \otimes \mathbf{E}_X + (V_Y + 1)\mathbf{e}_y \otimes \mathbf{E}_Y, \tag{2.2}$$

where $\mathbf{E}_X, \mathbf{E}_Y$ and $\mathbf{e}_x, \mathbf{e}_y$ represent the orthonormal basis in the reference and current configurations, respectively. Here we have chosen $\mathbf{E}_X = \mathbf{e}_x$ and $\mathbf{E}_Y = \mathbf{e}_y$.

Without loss of generality, we assume that this rectangle is composed of a compressible Murnaghan material whose strain energy function has the following form:

$$\Phi = \frac{\lambda}{2}(\mathrm{Tr}\mathbf{E})^2 + \mu(\mathrm{Tr}\mathbf{E}^2) + \nu_1(\mathrm{Tr}\mathbf{E})(\mathrm{Tr}\mathbf{E}^2) + \frac{\nu_2}{3}(\mathrm{Tr}\mathbf{E})^3 + \frac{\nu_4}{3}(\mathrm{Tr}\mathbf{E}^3), \tag{2.3}$$

where $\mathbf{E} = (\mathbf{F}^{\mathbf{T}}\mathbf{F} - \mathbf{I})/2$ is the Green strain tensor; λ and μ are known as the Lamé constants; ν_1, ν_2, and ν_4 are other constitutive constants; and Tr is the trace of a tensor.

The first Piola–Kirchhoff stress tensor Σ containing terms up to third-order material nonlinearity for an arbitrary strain energy function can be calculated by a formula provided in [15]:

$$\Sigma_{ij} = a^1_{jilk} d_{kl} + \frac{1}{2} a^2_{jilknm} d_{kl} d_{mn} + \frac{1}{6} a^3_{jilknmqp} d_{kl} d_{mn} d_{pq} + O\big(|d_{ij}|^4\big), \tag{2.4}$$

where $\mathbf{d} = \mathbf{F} - \mathbf{I}$; a^1_{jilk}, a^2_{jilknm}, and $a^3_{jilknmqp}$ are elastic moduli defined by

$$\begin{cases} a^1_{jilk} = \dfrac{\partial^2 \Phi}{\partial F_{ij} \partial F_{kl}}\bigg|_{\mathbf{F}=\mathbf{I}}, \quad a^2_{jilknm} = \dfrac{\partial^3 \Phi}{\partial F_{ij} \partial F_{kl} \partial F_{mn}}\bigg|_{\mathbf{F}=\mathbf{I}}, \\ a^3_{jilknmqp} = \dfrac{\partial^4 \Phi}{\partial F_{ij} \partial F_{kl} \partial F_{mn} \partial F_{pq}}\bigg|_{\mathbf{F}=\mathbf{I}}; \end{cases} \tag{2.5}$$

and $\mathbf{I}$ is the identity tensor corresponding to a natural configuration.

Here we study a static problem, and the field equations (neglecting the body force) are given by

$$\frac{\partial \Sigma_{xX}}{\partial X} + \frac{\partial \Sigma_{xY}}{\partial Y} = 0, \tag{2.6}$$

$$\frac{\partial \Sigma_{yX}}{\partial X} + \frac{\partial \Sigma_{yY}}{\partial Y} = 0. \tag{2.7}$$

Substituting (2.4) into (2.6) and (2.7), we have two complicated nonlinear partial differential equations (PDEs).

In addition to the above two governing equations, we assume that there is no lateral distributive loading on the lateral boundaries of the rectangle. Then the stress components Σ_{xY} and Σ_{yY} should vanish on the lateral boundaries. We have the following traction-free boundary conditions:

$$\Sigma_{xY} = 0, \quad \Sigma_{yY} = 0 \qquad \text{at } Y = \pm a. \tag{2.8}$$

We will study the solution bifurcations of the nonlinear PDEs (2.6) and (2.7) under (2.8) and some end conditions.

For the solution obtained if one of its deformation gradients has a finite jump across a curve in the rectangle, this solution should satisfy the jump conditions. These conditions require the force balance and the continuity of the displacements. Namely,

$$\Sigma^+ \mathbf{n} = \Sigma^- \mathbf{n} \quad \text{and} \quad \mathbf{F}^+ \mathbf{l} = \mathbf{F}^- \mathbf{l} \tag{2.9}$$

must hold on the curve of discontinuity. $\Sigma^\pm$ and $\mathbf{F}^\pm$ denote its limiting values at a point on the curve of discontinuity, and $\mathbf{n}$ is the unit normal and $\mathbf{l}$ are all vectors tangent to the curve.

3. Nondimensionalization and series-asymptotic reduction. It is difficult to study the nonlinear PDEs (2.6) and (2.7) together with the traction-free boundary conditions (2.8). But we can use the combined series-asymptotic expansion method to deal with this complicated system. This approach adopted here is similar to those used in [11, 16, 17, 18]. First we introduce a new set of dimensionless quantities through the following suitable scalings:

$$U = hu, \quad V = hv, \quad X = \bar{x}l, \quad Y = \bar{y}l, \quad \varepsilon = \frac{h}{l}, \quad \nu = \frac{a^2}{l^2}, \tag{3.1}$$

where h is the characteristic axial displacement, which can be regarded as the reduction of the distance between the ends, and ε is treated as a small parameter since here the deformation is considered to be small. We assume that the rectangle is thin such that ν is small, say, $\nu < 0.07$; this implies that $a/l < 0.2646$, i.e., that the aspect ratio is less than 0.5292. For simplicity of notation, we will drop the bar from $\bar{x}$ and $\bar{y}$ hereafter.

After the above proper scalings, the original field equations and traction-free boundary conditions can be transformed into the following dimensionless equations:

$$\eta_0 u_{yy} + (1-\eta_0) v_{xy} + u_{xx} + \varepsilon \mathscr{D}_1(u,v) + \varepsilon^2 \mathscr{D}_2(u,v) = 0, \tag{3.2}$$

$$v_{yy} + (1-\eta_0) u_{xy} + \eta_0 v_{xx} + \varepsilon \mathscr{D}_3(u,v) + \varepsilon^2 \mathscr{D}_4(u,v) = 0, \tag{3.3}$$

$$\eta_0 u_y + \eta_0 v_x + \varepsilon \mathscr{D}_5(u,v) + \varepsilon^2 \mathscr{D}_6(u,v) = 0 \qquad \text{at } y = \pm\sqrt{\nu}, \tag{3.4}$$

$$v_y + (1-2\eta_0) u_x + \varepsilon \mathscr{D}_7(u,v) + \varepsilon^2 \mathscr{D}_8(u,v) = 0 \qquad \text{at } y = \pm\sqrt{\nu}, \tag{3.5}$$

where $\eta_0 = \frac{\mu}{\lambda+2\mu}$ and $\mathscr{D}_i$ $(i = 1, \ldots, 18)$ are operators of the corresponding functions, whose explicit expressions can be found in [19].

It is also hard to analyze (3.2)–(3.5) directly. In the following, by using series expansions and asymptotic reductions, we will obtain much simplified equations.

Since we consider the case that ν is small and $-\sqrt{\nu} \le y \le \sqrt{\nu}$, y is a small variable. We can see that the whole problem depends on two small parameters ε and ν, one small variable y, and one variable x. Assume that $u(x,y)$ and $v(x,y)$ are sufficiently smooth; then they have the following Taylor expansions in the neighborhood of $y=0$:

$$u(x,y) = u_0(x) + y^2 u_2(x) + y^4 u_4(x) + \cdots + \delta y(u_1(x) + y^2 u_3(x) + \cdots), \tag{3.6}$$

$$v(x,y) = \delta(v_0(x) + y^2 v_2(x) + y^4 v_4(x) + \cdots) + y(v_1(x) + y^2 v_3(x) + \cdots), \tag{3.7}$$

where δ is a parameter that is a measure of the deflection of the central axis. Since the purpose here is to deduce the critical load for buckling when there is a buckling instability and compare the values with those obtained from the Bernoulli–Euler beam theory, we consider the case that δ is small such that $\delta = o(\sqrt{\nu})$.

Substituting (3.6) and (3.7) into the boundary conditions (3.4) and (3.5), we can obtain the following four equations:

$$\mathscr{D}_9(u_0,u_1,u_2,u_3,v_0,v_1,v_2,v_3) + O(\nu^2, \varepsilon^2\nu, \varepsilon^2\delta^2) = 0, \tag{3.8}$$

$$\mathscr{D}_{10}(u_0,u_2,u_4,v_1,v_3) + O(\nu^2, \varepsilon^2\nu, \varepsilon\delta^2) = 0, \tag{3.9}$$

$$\mathscr{D}_{11}(u_0,u_2,v_1,v_3) + O(\nu^2, \varepsilon^2\nu, \varepsilon\delta^2) = 0, \tag{3.10}$$

$$\mathscr{D}_{12}(u_0,u_1,u_2,u_3,v_0,v_1,v_2,v_3,v_4) + O(\nu^2, \varepsilon^2\nu, \varepsilon^2\delta^2) = 0. \tag{3.11}$$

In these equations, if the $O(\nu^2, \varepsilon^2\nu, \varepsilon\delta^2, \varepsilon^2\delta^2)$ terms are omitted, there are ten unknowns $u_0, \ldots, u_4, v_0, \ldots, v_4$. To have a closed system, we need another six equations.

Substituting (3.6) and (3.7) into the field equation (3.2), the left-hand side becomes a series in y. All the coefficients of y^n $(n = 0, 1, 2, 3, \ldots)$ should be zero, and as a result we have a set of infinitely many equations. It turns out that the first three equations $(n = 0, 1, 2)$ contain only the above-mentioned ten unknowns by neglecting proper higher-order terms. These equations are

$$\mathscr{D}_{13}(u_2,v_1,u_0) + O(\varepsilon\delta^2) = 0, \tag{3.12}$$

$$\mathscr{D}_{14}(u_3,v_0,v_1,v_2,v_3,u_0,u_1,u_2) + O(\varepsilon^2\delta^2) = 0, \tag{3.13}$$

$$\mathscr{D}_{15}(u_4,v_1,v_3,u_0,u_2) + O(\varepsilon\delta^2) = 0. \tag{3.14}$$

Similarly, substituting (3.6) and (3.7) into another field equation (3.3), and from the coefficients of y^0, y^1, and y^2, we have

$$\mathscr{D}_{16}(v_2,v_0,v_1,u_0,u_1,u_2) + O(\varepsilon^2\delta^2) = 0, \tag{3.15}$$

$$\mathscr{D}_{17}(v_3,v_1,u_0,u_2) + O(\varepsilon\delta^2) = 0, \tag{3.16}$$

$$\mathscr{D}_{18}(v_4,v_0,v_1,v_2,v_3,u_0,u_1,u_2,u_3,u_4) + O(\varepsilon^2\delta^2) = 0. \tag{3.17}$$

Now the field equations (3.2)–(3.3) and the boundary conditions (3.4)–(3.5) are changed into a one-dimensional system of differential equations (3.8)–(3.17) for ten unknowns $u_0, \ldots, u_4$, $v_0, \ldots, v_4$ if we neglect $O(\nu^2, \varepsilon^2\nu, \varepsilon\delta^2, \varepsilon^2\delta^2)$ in (3.8)–(3.11) and $O(\varepsilon\delta^2, \varepsilon^2\delta^2)$ in (3.12)–(3.17). By using the perturbation method, we can solve u_2 from (3.12). Then, substituting it into (3.16), we can get v_3. Further we substitute

u_2 and v_3 into (3.14) and can get u_4. Similarly, we can obtain v_2, u_3, and v_4 from (3.15), (3.13), and (3.17), respectively.

Substituting u_2, v_3, u_4 into the boundary conditions (3.9) and (3.10) and further omitting $O(\varepsilon^2)$, we obtain two equations in terms of u_0 and v_1. Similarly, substituting u_2, v_3, u_4, v_2, u_3, and v_4 into the boundary conditions (3.8) and (3.11) and further omitting $O(\varepsilon\nu)$, we obtain two equations in terms of u_0, u_1, v_0, and v_1. The detailed derivations can be found in the above-mentioned report [19]. Then we can obtain four equations with four variables u_0, u_1, v_0, and v_1. They are

$$
\begin{aligned}
&(-1+2\eta_0)v_{1x} - u_{0xx} + \nu\left(\left(\frac{1}{2} - \frac{2\eta_0}{3}\right)v_{1xxx} + \left(\frac{1}{2} - \frac{\eta_0}{3}\right)u_{0xxxx}\right)\\
&+ \varepsilon\big(-\alpha_4 v_1 v_{1x} - \alpha_4 u_{0x} v_{1x} - \alpha_4 v_1 u_{0xx} - \alpha_5 u_{0x} u_{0xx} + \nu(\alpha_{34} v_{1x} v_{1xx} + \alpha_{35} u_{0xx} v_{1xx}\\
&\qquad + \alpha_{36} v_{1x} u_{0xxx} + \alpha_{37} u_{0xx} u_{0xxx} + \alpha_{38} v_1 v_{1xxx} + \alpha_{39} u_{0x} v_{1xxx} + \alpha_{40} v_1 u_{0xxxx}\\
&\qquad + \alpha_{41} u_{0x} u_{0xxxx})\big) = 0,
\end{aligned}
\tag{3.18}
$$

$$
\begin{aligned}
&v_1 + (1-2\eta_0)u_{0x} + \nu\left(\left(\frac{1}{2} - \eta_0\right)v_{1xx} + \frac{1}{2}u_{0xxx}\right)\\
&+ \varepsilon\left(\frac{1}{2}\alpha_5 v_1^2 + \alpha_4 v_1 u_{0x} + \frac{1}{2}\alpha_4 u_{0x}^2 + \nu(\alpha_{42} v_{1x}^2 + 2\alpha_{42} v_{1x} u_{0xx} + \alpha_{43} u_{0xx}^2 + \alpha_{42} v_1 v_{1xx}\right.\\
&\left.\qquad + \alpha_{42} u_{0x} v_{1xx} + \alpha_{42} v_1 u_{0xxx} + \alpha_{43} u_{0x} u_{0xxx})\right) = 0,
\end{aligned}
\tag{3.19}
$$

$$
\begin{aligned}
&\eta_0 u_1 + \eta_0 v_{0x} + \nu\left(\left(-\frac{3\eta_0}{2} + \eta_0^2\right)u_{1xx} + \left(\frac{\eta_0}{2} - \eta_0^2\right)v_{0xxx}\right)\\
&+ \varepsilon\big(\alpha_1 u_1 v_1 + \alpha_1 u_1 u_{0x} + \alpha_2 v_1 v_{0x} + \alpha_2 u_{0x} v_{0x}\big)\\
&+ \varepsilon^2\left(\alpha_6 u_1 v_1^2 + 2\alpha_7 u_1 v_1 u_{0x} + \alpha_6 u_1 u_{0x}^2 + \frac{3}{2}(\alpha_1 - 1)v_1^2 v_{0x}\right.\\
&\left.\qquad + \alpha_8 v_1 u_{0x} v_{0x} + \frac{3}{2}(\alpha_1 - 1)u_{0x}^2 v_{0x}\right) = 0,
\end{aligned}
\tag{3.20}
$$

$$
\begin{aligned}
&-\eta_0 u_{1x} - \eta_0 v_{0xx} + \nu\left(\left(\frac{\eta_0}{2} - \frac{\eta_0^2}{3}\right)u_{1xxx} + \left(-\frac{\eta_0}{6} + \frac{\eta_0^2}{3}\right)v_{0xxxx}\right)\\
&+ \varepsilon\big(-\alpha_2 v_1 u_{1x} - \alpha_2 u_{0x} u_{1x} - \alpha_2 u_1 v_{1x} - \alpha_1 v_{0x} v_{1x} - \alpha_2 u_1 u_{0xx}\\
&\qquad - \alpha_1 v_{0x} u_{0xx} - \alpha_1 v_1 v_{0xx} - \alpha_1 u_{0x} v_{0xx}\big)\\
&+ \varepsilon^2\left(-\frac{3}{2}(\alpha_1 - 1)v_1^2 u_{1x} - \alpha_8 v_1 u_{0x} u_{1x} - \frac{3}{2}(\alpha_1 - 1)u_{0x}^2 u_{1x} - 3(\alpha_1 - 1)u_1 v_1 v_{1x}\right.\\
&\qquad - \alpha_8 u_1 u_{0x} v_{1x} - 2\alpha_6 v_1 v_{0x} v_{1x} - 2\alpha_7 u_{0x} v_{0x} v_{1x} - \alpha_8 u_1 v_1 u_{0xx}\\
&\qquad - 3(\alpha_1 - 1)u_1 u_{0x} u_{0xx} - 2\alpha_7 v_1 v_{0x} u_{0xx} - 2\alpha_6 u_{0x} v_{0x} u_{0xx} - \alpha_6 v_1^2 v_{0xx}\\
&\qquad \left. - 2\alpha_7 v_1 u_{0x} v_{0xx} - \alpha_6 u_{0x}^2 v_{0xx}\right) = 0,
\end{aligned}
\tag{3.21}
$$

where α_i $(i = 1, \ldots, 48)$ are constants related to material constants, whose expressions are given in [19]. It can be seen that (3.18) and (3.19) are two equations with two variables v_1 and u_0, and (3.20) and (3.21) are two equations with four variables v_1, u_0, u_1, and v_0. (Note: in (3.20) and (3.21) we keep $O(\varepsilon^2)$ terms in order to consider the nonlinear effect of the axial strain on the possible deflection.) We also notice that

both (3.18) and (3.21) can be integrated once. Then we obtain the following two equations:

$$
\begin{aligned}
&(1-2\eta_0)v_1+u_{0x}+\nu\left(\left(-\frac{1}{2}+\frac{2\eta_0}{3}\right)v_{1xx}+\left(-\frac{1}{2}+\frac{\eta_0}{3}\right)u_{0xxx}\right)\\
&+\varepsilon\left(\frac{1}{2}\alpha_4v_1^2+\alpha_4v_1u_{0x}+\frac{1}{2}\alpha_5u_{0x}^2+\nu\left((\alpha_{39}-\alpha_{35})u_{0xx}v_{1x}-\alpha_{39}u_{0x}v_{1xx}+\alpha_{40}v_1u_{0xxx}\right.\right.\\
&\left.\left.-\frac{1}{2}(\alpha_{34}-\alpha_{38})v_{1x}^2-\alpha_{38}v_1v_{1xx}-\frac{1}{2}(\alpha_{37}-\alpha_{41})u_{0xx}^2-\alpha_{41}u_{0x}u_{0xxx}\right)\right)=A,
\end{aligned}
\tag{3.22}
$$

$$
\begin{aligned}
&\eta_0u_1+\eta_0v_{0x}+\nu\left(\left(-\frac{\eta_0}{2}+\frac{\eta_0^2}{3}\right)u_{1xx}+\left(\frac{\eta_0}{6}-\frac{\eta_0^2}{3}\right)v_{0xxx}\right)\\
&+\varepsilon\Big(\alpha_2u_1v_1+\alpha_2u_1u_{0x}+\alpha_1v_1u_{0x}+\alpha_1u_{0x}v_{0x}\Big)\\
&+\varepsilon^2\left(\frac{3}{2}(\alpha_1-1)u_1v_1^2+\alpha_8u_1v_1u_{0x}+\frac{3}{2}(\alpha_1-1)u_1u_{0x}^2\right.\\
&\left.+\alpha_6v_1^2v_{0x}+2\alpha_7v_1u_{0x}v_{0x}+\alpha_6u_{0x}^2v_{0x}\right)=B,
\end{aligned}
\tag{3.23}
$$

where A and B are two integration constants.

By eliminating v_{1xx} terms from (3.19) and (3.22), and using a perturbation expansion, we obtain

$$
v_1=(-1+2\eta_0)u_{0x}+\alpha_{44}\nu u_{0xxx}+\varepsilon(\alpha_{45}u_{0x}^2+\nu(\alpha_{46}u_{0xx}^2+\alpha_{47}u_{0x}u_{0xxx}))
\tag{3.24}
$$

and

$$
u_{0x}-\frac{1}{3}\nu u_{0xxx}+\varepsilon(D_1u_{0x}^2+\nu(-D_2u_{0xx}^2-2D_2u_{0x}u_{0xxx}))=\frac{A}{4(1-\eta_0)\eta_0},
\tag{3.25}
$$

where D_1 and D_2 are constants related to constitutive constants.

Similarly, from (3.20) and (3.23), we obtain

$$
u_1=-v_{0x}+2\nu(\eta_0-1)v_{0xxx}+\varepsilon\big(2(1-\eta_0)u_{0x}v_{0x}\big)+\varepsilon^2\big(\alpha_{48}u_{0x}^2v_{0x}\big)
\tag{3.26}
$$

and

$$
-\frac{1}{3}\nu v_{0xxx}+\varepsilon u_{0x}v_{0x}+\varepsilon^2(D_1-1)u_{0x}^2v_{0x}=\frac{B}{4(1-\eta_0)\eta_0}.
\tag{3.27}
$$

In order to find the physical meanings of the two integration constants A and B, we consider the axial resultant force $T=\int_{-a}^{a}\Sigma_{xX}dY$ and the shear resultant force $Q=\int_{-a}^{a}\Sigma_{yX}dY$. After expressing Σ_{xX} and Σ_{yX} in terms of u_0 and v_1 and carrying out the integration, we find that $\frac{T}{2a\varepsilon(\lambda+2\mu)}=A$ and $\frac{Q}{2a\varepsilon\delta(\lambda+2\mu)}=B$; i.e., $\frac{T}{2a\varepsilon\hat{E}}=\frac{A}{4(1-\eta_0)\eta_0}$ and $\frac{Q}{2a\varepsilon\delta\hat{E}}=\frac{B}{4(1-\eta_0)\eta_0}$, where $\hat{E}=\frac{4\mu(\lambda+\mu)}{\lambda+2\mu}$ is an elastic modulus. Now we let $\gamma=\frac{T}{2a\hat{E}}$ and $q=\frac{Q}{2a\hat{E}}$. Hence γ and q are the nondimensionalized average axial and shear resultant forces, respectively. Then, from (3.25) and (3.27), we have

$$
\begin{cases}
W+D_1W^2-\dfrac{a^2}{3}W_{XX}-D_2a^2(W_X^2+2WW_{XX})=\gamma,\\
\big(W+(D_1-1)W^2\big)G-\dfrac{a^2}{3}G_{XX}=q,
\end{cases}
\tag{3.28}
$$

where the original dimensional variables $W(X)=\varepsilon u_{0x}$ and $G(X)=\varepsilon\delta v_{0x}$ are used.

Now we have finally obtained two decoupled nonlinear ODEs, $(3.28)_1$ and $(3.28)_2$. In the next section, we will derive the same two equations by using the variational principle.

4. Euler–Lagrange equations. In this section, we will derive the same decoupled equations as in (3.28) by using the variational principle. From (2.3) we can get the expression of the strain energy Φ up to fourth-order nonlinearity (which implies that the stress components are up to third-order nonlinearity, in agreement with our previous derivations). The average total strain energy per unit length over a cross-line is given by $\bar{\Phi} = \frac{1}{2a}\int_{-a}^{a} \Phi dY$. By using the results in the previous sections, we can express $\bar{\Phi}$ in terms of u_0, u_1, v_0, and v_1. By further using (3.24) and (3.26) and omitting higher-order terms, we obtain

$$\bar{\Phi} = \hat{E}\left(\frac{1}{2}W^2 - \frac{1}{6}a^2 WW_{XX} + \frac{1}{3}D_1 W^3 + a^2\left(F_1 WW_X^2 + F_2 W^2 W_{XX}\right)\right.$$
$$\left. + \frac{1}{6}a^2 G_X^2 + \frac{1}{2}WG^2 + \frac{1}{2}(D_1 - 1)W^2 G^2\right), \tag{4.1}$$

where

$$F_1 = \frac{8 - 19\eta_0 + 10\eta_0^2 + 6(-2 + 3\eta_0)D_2 + 2(-6 + 7\eta_0)D_1}{12 - 24\eta_0}, \tag{4.2}$$

$$F_2 = \frac{8 - 19\eta_0 + 10\eta_0^2 - 6\eta_0 D_2 + 2(-6 + 7\eta_0)D_1}{24 - 48\eta_0}. \tag{4.3}$$

The average total potential energy is then given by

$$\Psi = \int_0^l \bar{\Phi} dX - \hat{E}\int_0^l \gamma W dX - \hat{E}\int_0^l qG dX. \tag{4.4}$$

So the Lagrangian is given by

$$L = \bar{\Phi} - \hat{E}\gamma W - \hat{E}qG. \tag{4.5}$$

Further, by the variational principle, we have the following Euler–Lagrange equations:

$$\begin{cases} \dfrac{\partial L}{\partial W} - \dfrac{d}{dX}\dfrac{\partial L}{\partial W_X} + \dfrac{d^2}{dX^2}\dfrac{\partial L}{\partial W_{XX}} = 0, \\ \dfrac{\partial L}{\partial G} - \dfrac{d}{dX}\dfrac{\partial L}{\partial G_X} = 0. \end{cases} \tag{4.6}$$

If we omit $O(\varepsilon^2\delta^2)$ in $(4.6)_1$, we have two equations which are the same as (3.28).

These are two decoupled nonlinear ODEs, which we refer to as the asymptotic normal form equations of the original nonlinear PDEs. After imposing proper end conditions, we will study solution bifurcations of this system. The solution bifurcations of the original complicated nonlinear PDEs can be studied through those of the asymptotic normal form equations.

5. Clamped boundary conditions at two ends. In this section, we consider the asymptotic simplifications of the clamped boundary conditions. As illustrated in Figure 2.1, two thin parts of the rectangle are clamped to two rigid bodies. The bottom is fixed, and the top is slidably supported. We will consider the rectangle

between the two dashed lines. Without loss of generality, hereafter we take the length of the rectangle to be 1, and then $2a$ is the aspect ratio (width over length) of the rectangle. Then we can propose the following asymptotic boundary conditions for the clamped ends:

(1) For the points A, B, C, D, there is no lateral movement. So we have $V(0, \pm a) = 0$ and $V(1, \pm a) = 0$. From the series expansion of V, we have

$$V(0, \pm a) = h(\delta v_0(0) \pm a(v_1(0) + a^2 v_3(0))) + O(h\delta a^2, ha^5) = 0. \tag{5.1}$$

By omitting $O(h\delta a^2, ha^5)$, we have

$$v_0(0) = 0 \quad \text{and} \quad v_1(0) + a^2 v_3(0) = 0. \tag{5.2}$$

From the perturbation expansions of v_1 and v_3 and (3.25), we can reduce $(5.2)_2$ to

$$\frac{1 - 6\alpha_{44}}{2}\gamma + \frac{-3 + 4\eta_0 + 6\alpha_{44}}{2}W(0) + \left(D_1 \frac{-1 + 6\alpha_{44}}{2} + \alpha_{45}\right) W^2(0) = 0. \tag{5.3}$$

Then we have

$$W(0) = \Delta_1, \tag{5.4}$$

where $\Delta_1 = \frac{3 - 4\eta_0 - 6\alpha_{44} - \sqrt{(3 - 4\eta_0 - 6\alpha_{44})^2 + 4\gamma(1 - 6\alpha_{44})(D_1(1 - 6\alpha_{44}) - 2\alpha_{45})}}{2(2\alpha_{45} - D_1(1 - 6\alpha_{44}))}$ is a small negative number depending on the external force γ and constitutive constants. We can see that $\Delta_1 = 0$ when $\gamma = 0$.

Similarly, we can obtain

$$v_0(1) = 0 \quad \text{and} \quad W(1) = \Delta_1. \tag{5.5}$$

(2) For the points A and B, there is no axial movement which leads to the condition $U(0, \pm a) = 0$. From the series expansion of U, we have

$$U(0, \pm a) = h(u_0(0) \pm \delta a(u_1(0) + a^2 u_3(0))) + O(ha^2, h\delta a^5). \tag{5.6}$$

By omitting $O(ha^2, h\delta a^5)$, we have

$$u_0(0) = 0 \quad \text{and} \quad u_1(0) + a^2 u_3(0) = 0. \tag{5.7}$$

From the perturbation expansions of u_1, u_3, and (3.27), we can reduce $(5.7)_2$ to

$$G(0) = \Delta_2 = qK, \tag{5.8}$$

where $K = \frac{\frac{9}{2} - 5\eta_0}{1 - (-\frac{5}{2} + 3\eta_0)\Delta_1 - (\frac{9}{2} - 5\eta_0 + \alpha_{48} + (-\frac{9}{2} + 5\eta_0)D_1)\Delta_1^2}$.

(3) The points C and D should have the same axial displacement, i.e., $U(1, a) = U(1, -a)$, which leads to the following condition:

$$G(1) = \Delta_2. \tag{5.9}$$

Now we list the asymptotic end conditions for the asymptotic normal form equations (3.28):

$$v_0 = 0, \quad G = \Delta_2, \quad u_0 = 0, \quad W = \Delta_1 \quad \text{at } X = 0, \tag{5.10}$$

$$v_0 = 0, \quad G = \Delta_2, \quad W = \Delta_1 \quad \text{at } X = 1. \tag{5.11}$$

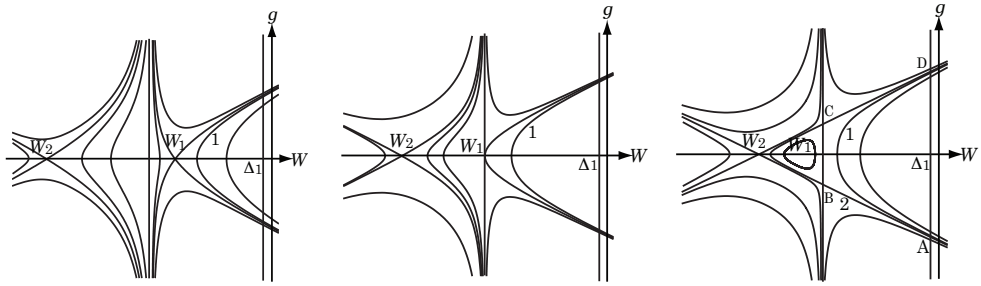

(a) (b) (c)

FIG. 6.1. *Phase planes for different γ values:* (a) $\gamma_p < \gamma < 0$; (b) $\gamma = \gamma_p$; (c) $\gamma_c \le \gamma < \gamma_p$ *and* $-\frac{1}{4D_1} < \gamma < \gamma_c$.

6. Bifurcation analysis. In this section we will undertake some bifurcation analysis of the asymptotic normal form equations (3.28). An equation similar to $(3.28)_1$ has been derived by Dai and Wang in [10, 11] for compressions of a cylinder, and some bifurcation results were obtained. Here we will use these results to study our problem. It is found that there are two different kinds of bifurcation phenomena for chosen material constants. One is that there is a bifurcation to a corner-like profile only when the aspect ratio is relatively large, which is a barrelling instability. Another is that there are bifurcations to the buckled profiles only when the aspect ratio is relatively small.

6.1. Barrelling instability: Bifurcation to a corner-like profile. First we can rewrite $(3.28)_1$ as

$$\begin{cases} W_X = g, \\ g_X = \dfrac{W + D_1 W^2 - a^2 D_2 g^2 - \gamma}{a^2(\frac{1}{3} + 2D_2 W)}. \end{cases} \tag{6.1}$$

The vector field of system (6.1) has a denominator term, which is zero at $W = -\frac{1}{6D_2}$, and thus it is a singular ODE system. Equation (6.1) with $(5.10)_4$ and $(5.11)_3$ form a boundary-value problem of a singular system. In this case, the detailed analysis of this singular dynamical system is almost the same as that in [11]. From (3.25), it can be seen that the arising of the denominator D_2-term is due to the coupling of the material nonlinearity (measured by ε) and the geometrical size (measured by ν). Here we again point out that this is due to the interaction between the material nonlinearity and geometrical size which causes the bifurcation to the formation of a corner-like profile, as noted in [10, 11].

We concentrate on the case of $3D_2 > D_1 > 0$, for which it is sufficient to illustrate the bifurcation to a corner-like profile. The equilibrium points of the system are given by

$$g = 0, \quad \gamma = W + D_1 W^2. \tag{6.2}$$

In the $W - g$ phase plane, there is a vertical singular line $W = -\frac{1}{6D_2}$. There are three different phase planes as γ varies, which are shown in Figure 6.1, where γ_c will

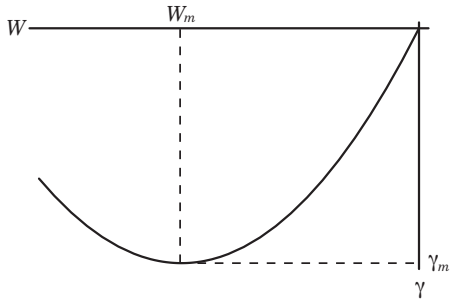

FIG. 6.2. *Stress-strain plot.*

be defined later and γ_p is calculated from $(6.2)_2$ for $W = -\frac{1}{6D_2}$, i.e.,

$$\gamma_p = D_1\left(\frac{-1}{6D_2}\right)^2 - \frac{1}{6D_2}. \tag{6.3}$$

The one-dimensional stress-strain relationship is given in Figure 6.2. Without loss of generality we let $a = 0.25$, $D_1 = 2.4$, $D_2 = 0.88$, and the Poisson ratio $\sigma = \frac{\lambda}{2(\lambda+\mu)} = 0.495$ to get the graphical results. Then $\gamma_p = -0.103306$. For a trajectory in a phase plane to be a solution of the boundary-value problem of (6.1), $(5.10)_4$, and $(5.11)_3$, a necessary and sufficient condition is that it contact the vertical line $W = \Delta_1$ twice and its X-interval be exactly equal to 1. Next, we discuss the solution(s) in each phase plane separately.

Case (a), $\gamma_p < \gamma < 0$ (see Figure 6.1(a)). In this case there is a unique solution denoted by trajectory 1. This trajectory crosses the W-axis at $(W_0, 0)$ in the corresponding phase plane. The solution expression is given in the following by referring to [20]:

(6.4)

$$X = \begin{cases} \dfrac{1}{2} - \dfrac{1}{\beta}\dfrac{2}{\sqrt{(W_0+\frac{1}{6D_2})(E_2-E_1)}}\left((W_0-E_2)\Pi\left(\theta, \dfrac{W_0-E_1}{E_2-E_1}, m\right)\right. \\ \qquad\qquad \left. + \left(E_2 + \dfrac{1}{6D_2}\right)F(\theta, m)\right), \qquad 0 \le X \le \dfrac{1}{2}, \\ \dfrac{1}{2} + \dfrac{1}{\beta}\dfrac{2}{\sqrt{(W_0+\frac{1}{6D_2})(E_2-E_1)}}\left((W_0-E_2)\Pi\left(\theta, \dfrac{W_0-E_1}{E_2-E_1}, m\right)\right. \\ \qquad\qquad \left. + \left(E_2 + \dfrac{1}{6D_2}\right)F(\theta, m)\right), \qquad \dfrac{1}{2} \le X \le 1, \end{cases}$$

where Π and F are the elliptic integral of the third kind and the first kind, respectively, and

$$E_1 = \frac{-3 - 2D_1W_0 - \sqrt{3(3 + 16\gamma D_1 - 4D_1W_0 - 4D_1^2W_0^2)}}{4D_1}, \tag{6.5}$$

$$E_2 = \frac{-3 - 2D_1W_0 + \sqrt{3(3 + 16\gamma D_1 - 4D_1W_0 - 4D_1^2W_0^2)}}{4D_1}, \tag{6.6}$$

(6.7)

$$\beta = \frac{1}{a}\sqrt{\frac{D_1}{3D_2}}, \quad \theta = \arcsin\sqrt{\frac{(E_2-E_1)(W-W_0)}{(W_0-E_1)(W-E_2)}}, \quad m = \sqrt{\frac{(E_2+\frac{1}{6D_2})(W_0-E_1)}{(W_0+\frac{1}{6D_2})(E_2-E_1)}}.$$

As $W=\Delta_1$ at $X=0$, W_0 is determined by

$$\frac{1}{2}=\frac{1}{\beta}\frac{2}{\sqrt{(W_0+\frac{1}{6D_2})(E_2-E_1)}}\left((W_0-E_2)\Pi\left(\theta_0,\frac{W_0-E_1}{E_2-E_1},m\right)+\left(E_2+\frac{1}{6D_2}\right)F(\theta_0,m)\right),$$

where $\theta_0=\arcsin\sqrt{\frac{(E_2-E_1)(\Delta_1-W_0)}{(W_0-E_1)(\Delta_1-E_2)}}$.

Case (b), $\gamma=\gamma_p$ (see Figure 6.1(b)). In this case, there is a trajectory tangent to the singular line in the phase plane, as shown in Figure 6.1(b). There is a unique solution denoted by trajectory 1 in the phase plane. Trajectory 1 contacts the W-axis at $(W_0,0)$. The solution expression is given by

$$X=\begin{cases}\frac{1}{2}-\frac{1}{\beta}\frac{2(W_0+\frac{1}{6D_2})}{\sqrt{(W_0-E_2)(\frac{-1}{6D_2}-E_1)}}\Pi\left(\theta,\frac{W_0-E_1}{-\frac{1}{6D_2}-E_1},m\right), & 0\le X\le\frac{1}{2},\\ \frac{1}{2}+\frac{1}{\beta}\frac{2(W_0+\frac{1}{6D_2})}{\sqrt{(W_0-E_2)(\frac{-1}{6D_2}-E_1)}}\Pi\left(\theta,\frac{W_0-E_1}{-\frac{1}{6D_2}-E_1},m\right), & \frac{1}{2}\le X\le 1,\end{cases}\tag{6.8}$$

where E_1 and E_2 are the same as (6.5) and (6.6), respectively, and

$$\theta=\arcsin\sqrt{\frac{(\frac{-1}{6D_2}-E_1)(W-W_0)}{(W_0-E_1)(W+\frac{1}{6D_2})}},\qquad m=\sqrt{\frac{(\frac{-1}{6D_2}-E_2)(W_0-E_1)}{(W_0-E_2)(\frac{-1}{6D_2}-E_1)}}.\tag{6.9}$$

As $W=\Delta_1$ at $X=0$, W_0 is determined by

$$\frac{1}{2}=\frac{1}{\beta}\frac{2(W_0+\frac{1}{6D_2})}{\sqrt{(W_0-E_2)(\frac{-1}{6D_2}-E_1)}}\Pi\left(\theta_0,\frac{W_0-E_1}{-\frac{1}{6D_2}-E_1},m\right),\tag{6.10}$$

where

$$\theta_0=\arcsin\sqrt{\frac{(-\frac{1}{6D_2}-E_1)(\Delta_1-W_0)}{(W_0-E_1)(\Delta_1+\frac{1}{6D_2})}}.$$

Case (c), $\gamma_c<\gamma<\gamma_p$ (see Figure 6.1(c)). There is a unique solution represented by trajectory 1. It contacts the W-axis at $(W_0,0)$. This solution can be expressed in the following form:

$$X=\begin{cases}-\frac{1}{\beta}\int_{\Delta_1}^{W}\sqrt{\frac{W+\frac{1}{6D_2}}{(W-W_0)(W^2+t_1W+t_2)}}dW, & 0\le X\le\frac{1}{2},\\ \frac{1}{2}+\frac{1}{\beta}\int_{W_0}^{W}\sqrt{\frac{W+\frac{1}{6D_2}}{(W-W_0)(W^2+t_1W+t_2)}}dW, & \frac{1}{2}\le X\le 1,\end{cases}\tag{6.11}$$

where $t_1=\frac{6\gamma+3W_0+2D_1W_0^2}{2D_1}$ and $t_2=\frac{3+2D_1W_0}{2D_1}$. Further, W_0 is determined by the following equation:

$$\frac{1}{2}=-\frac{1}{\beta}\int_{\Delta_1}^{W_0}\sqrt{\frac{W+\frac{1}{6D_2}}{(W-W_0)(W^2+t_1W+t_2)}}dW.\tag{6.12}$$

Case (d), $\gamma = \gamma_c$ (see Figure 6.1(c)). We define γ_c to be the critical stress value such that when $\gamma = \gamma_c$, trajectory 2 in Figure 6.1(c)—which starts from A, goes to B, jumps from B to C, and finally arrives at D—is also a solution. In this case, there is another solution indexed by 1 in Figure 6.1(c). Trajectory 1 contacts the W-axis at $(W_0, 0)$, and its solution is also expressed by (6.11), and W_0 is determined by (6.12). We find that for this solution the value of W_{XX} at $X = 0.5$ is relatively small. Indeed, for $\gamma = \gamma_c$, $W_{XX} = 1.68199$ at $X = 0.5$.

The solution expression corresponding to trajectory 2 is given by

(6.13)
$$W(X) = \begin{cases} E_2 + (E_2 - E_1)\sinh^2\dfrac{1}{2}\left(2\,\mathrm{arcsinh}\sqrt{\dfrac{-\frac{1}{6D_2} - E_2}{-E_1 + E_2}} + \beta\left(\dfrac{1}{2} - X\right)\right), \ 0 \le X \le \dfrac{1}{2}, \\ E_2 + (E_2 - E_1)\sinh^2\dfrac{1}{2}\left(2\,\mathrm{arcsinh}\sqrt{\dfrac{-\frac{1}{6D_2} - E_2}{-E_1 + E_2}} + \beta\left(X - \dfrac{1}{2}\right)\right), \ \dfrac{1}{2} \le X \le 1, \end{cases}$$

where

$$E_1 = \frac{D_1 - 9D_2 - \sqrt{3(-D_1^2 + 27D_2^2 + 6D_1D_2(1 + 24\gamma D_2))}}{12D_1D_2}, \tag{6.14}$$

$$E_2 = \frac{D_1 - 9D_2 + \sqrt{3(-D_1^2 + 27D_2^2 + 6D_1D_2(1 + 24\gamma D_2))}}{12D_1D_2}. \tag{6.15}$$

As $W = \Delta_1$ at $X = 0$, we have

$$\frac{1}{2} = \frac{1}{\beta}\left(2\,\mathrm{arcsinh}\sqrt{\frac{\Delta_1 - E_2}{E_1 - E_2}} - 2\,\mathrm{arcsinh}\sqrt{\frac{-\frac{1}{6D_2} - E_2}{-E_1 + E_2}}\right), \tag{6.16}$$

which determines the value of γ_c. For the previously chosen parameters, we find $\gamma_c = -0.1038086$.

Alternatively, (6.13) can be rewritten as

$$W(X) = E_2 + (E_2 - E_1)\sinh^2\frac{1}{2}\left(2\,\mathrm{arcsinh}\sqrt{\frac{-\frac{1}{6D_2} - E_2}{-E_1 + E_2}} + \beta\left|\frac{1}{2} - X\right|\right). \tag{6.17}$$

This is a nonsmooth solution whose first-order derivative at $X = 0.5$ does not exist. This nonsmooth solution is a weak solution of the singular ODE system according to the definition given in [21]. However, for this solution the jump conditions (2.9) cannot be satisfied exactly, and we shall not take it as one solution of the field equations. We intend to find the smooth solution which has a very large second-order derivative value at one point.

Case (e), $-\frac{1}{4D_1} < \gamma < \gamma_c$ (see Figure 6.1(c)). When $|\gamma|$ is slightly larger than $|\gamma_c|$, there are two solutions, both of which can be indexed by 1. Equation (6.11) provides the expression for both of them. We denote the crossing points with the W-axis of the two solution trajectories by $(\tilde{W}_0, 0)$ and $(W_0, 0)$, respectively, and $\tilde{W}_0$ and W_0 can be determined by (6.12). We notice that for one of them the point $(\tilde{W}_0, 0)$ is very close to the singular line, which represents a sharp-crest profile with a large second-order derivative W_{XX} at $X = 0.5$.

For $\gamma = -0.103809 < \gamma_c = -0.1038086$, we find that $W_0 = -0.182968$ and $\tilde{W}_0 = -0.189393$, which is very close to the singular line $V = -\frac{1}{6D_2} = -0.189394$. The corresponding average total potential energy values for the two solutions are, respectively,

$$\Psi = -5.48367 \times 10^{-3}\hat{E}, \qquad \tilde{\Psi} = -5.48513 \times 10^{-3}\hat{E}, \tag{6.18}$$

which are obtained from (4.4) ($G = 0$ for a barrelling instability).

Trajectory 1 with $\tilde{W}_0$ has a smaller energy value and is thus an energetically preferred solution. For this solution, we find that $W_{XX} = 115.8$ at $Z = 0.5$, indeed a very large value. The solution curve corresponding to this trajectory is shown in Figure 6.3(a). The corresponding lateral boundary profile of the rectangle and the shape of the rectangle in the current configuration are shown in Figures 6.3(b) and (c), respectively. The vertical scale in Figure 6.3(b) is significantly enlarged to reflect the large second-order derivative in the middle. In Figure 6.3(c), the same scale is used for both the x- and y-axes, and we can see that the profile looks like what one would expect for a barrelled state.

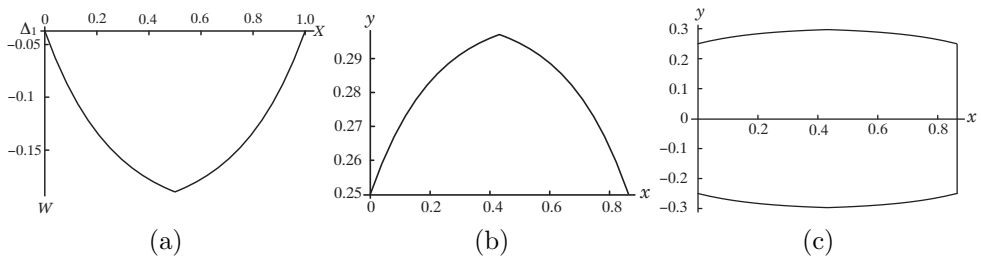

(a) (b) (c)

FIG. 6.3. (a) *Plot of W with a large second-order derivative.* (b) *Profile of the lateral boundary $Y = a$ of the rectangle (x and y are the current coordinates).* (c) *Shape of the barrelled rectangle in the current configuration.*

By considering the other values of a, we find that when $0.376 < 2a < 0.5292$ there is a bifurcation to the corner-like profile. Thus, for the material constants chosen here, 0.376 is a lower bound of the aspect ratio for the barrelling instability. We also point out that, for the barrelling solution obtained, we find that there is no nontrivial solution for $(3.28)_2$ together with boundary conditions $(5.10)_1$, $(5.10)_2$, $(5.11)_1$, and $(5.11)_2$. This implies that no buckling will occur after the barrelling.

Remark. The solutions obtained in this section satisfy $W_m \le W \le 0$ (cf. Figure 6.2); i.e., W is in the "hardening" branch.

6.2. Buckling instability: Bifurcation to a buckled profile. In this section, we discuss the bifurcation phenomenon of buckling. Since the solutions for $W(X)$ have been obtained in the previous section, in the following discussion we concentrate on $(3.28)_2$. This equation together with the clamped boundary conditions $(5.10)_1$, $(5.10)_2$, $(5.11)_1$, and $(5.11)_2$ compose an eigenvalue problem, in which γ, contained in W, is the eigenvalue and G is the corresponding eigenfunction.

For $W(X)$ given in cases (a) to (e) in the previous section, we define $f(X) = W(X) + (D_1 - 1)W^2(X)$. By letting $\tau = \frac{a}{\sqrt{3}}$, equation $(3.28)_2$ can be written as

$$\tau^2 G_{XX} - f(X)G = -q. \tag{6.19}$$

Since we set the length $l = 1$ and we are considering a thin rectangle, τ is a small parameter. We can obtain two linearly independent complementary solutions of the

corresponding homogeneous equation by the WKB method. For an introduction of the WKB method, we refer to [22].

Then, by the method of variation of parameters, a particular solution (to leading order) of (6.19) can be found. Then the general solution of (6.19), to leading order, is given by

$$G(X,\tau) = C_1(-f(X))^{-\frac{1}{4}}\cos\int_0^X \frac{\sqrt{-f(t)}}{\tau}dt + C_2(-f(X))^{-\frac{1}{4}}\sin\int_0^X \frac{\sqrt{-f(t)}}{\tau}dt$$
$$+\frac{q}{\tau}\int_0^X (f(s)f(X))^{-\frac{1}{4}}\sin\int_X^s \frac{\sqrt{-f(t)}}{\tau}dtds, \tag{6.20}$$

where C_1 and C_2 are two constants.

By the condition $(5.10)_2$, we have $C_1 = qK(-f(1))^{\frac{1}{4}}$. And, from the conditions $(5.10)_1$, $(5.11)_1$, and $(5.11)_2$, we have

$$\begin{cases} C_2A_1 + \dfrac{q}{\tau}A_2 = 0, \\ C_2B_1 + \dfrac{q}{\tau}B_2 = 0, \end{cases} \tag{6.21}$$

where

$$\begin{cases} A_1 = (-f(1))^{-\frac{1}{4}}\sin\displaystyle\int_0^1 \frac{\sqrt{-f(t)}}{\tau}dt, \\ A_2 = K\tau\left(\cos\displaystyle\int_0^1 \frac{\sqrt{-f(t)}}{\tau}dt - 1\right) + \displaystyle\int_0^1 (f(s)f(1))^{-\frac{1}{4}}\sin\int_1^s \frac{\sqrt{-f(t)}}{\tau}dtds, \\ B_1 = \displaystyle\int_0^1 (-f(X))^{-\frac{1}{4}}\sin\int_0^X \frac{\sqrt{-f(t)}}{\tau}dtdX, \\ B_2 = K\tau(-f(1))^{\frac{1}{4}}\displaystyle\int_0^1 (-f(X))^{-\frac{1}{4}}\cos\int_0^X \frac{\sqrt{-f(t)}}{\tau}dtdX \\ \qquad + \displaystyle\int_0^1\int_0^X (f(s)f(X))^{-\frac{1}{4}}\sin\int_X^s \frac{\sqrt{-f(t)}}{\tau}dtdsdX. \end{cases} \tag{6.22}$$

To obtain nontrivial solutions, we need the determinant of the coefficient matrix of (6.21) to be zero, i.e.,

$$A_1B_2 - A_2B_1 = 0. \tag{6.23}$$

This is the algebraic equation for determining the eigenvalue γ.

In Figures 6.4(a) and (b), we plot the curves of the left-hand side of (6.23) for $a = 0.045$ and $a = 0.06$. The stress values at intersection points of the curve with the γ-axis are the critical stress values. There are three critical stress values when $a = 0.045$ and two when $a = 0.06$. It is expected that more critical stress values will appear when the aspect ratio $2a$ is smaller.

In Figure 6.4(c) we give the curve for $a = 0.25$. It can be seen that there is no bifurcation point to buckling before and after the barrelling to the corner-like profile occurs. Actually, when $a > 0.0955$, there is no bifurcation to buckling. Thus, for the material constants chosen here, 0.191 is the upper bound of the aspect ratio for the buckling instability.

Note that the elastic instability of the compression of a bar was first studied by Euler in 1744 and then by Lagrange and Bernoulli (see [23]). A historical statement

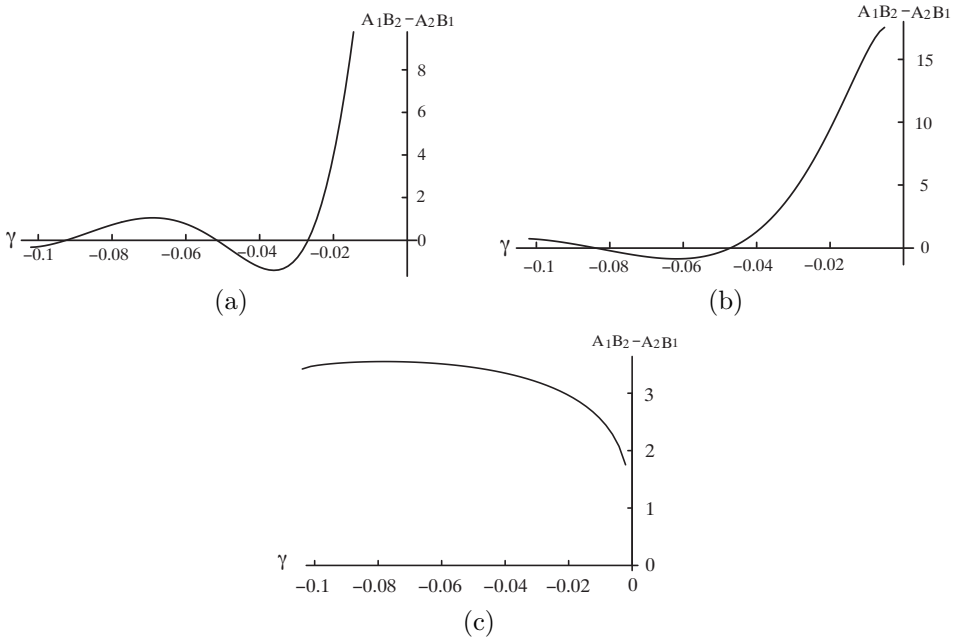

FIG. 6.4. *The bifurcation curves when* (a) $a = 0.045$; (b) $a = 0.06$; (c) $a = 0.25$.

about Euler's derivation can also be found in [23]. According to the Bernoulli–Euler constitutive equation, which says that the bending moment is linear in the change of curvature (see Antman [24]), a fourth-order linear ODE for the transverse displacement of a slender rectangle can be obtained,

$$\hat{E}Iu^{(4)}(s) + \Lambda u''(s) = 0, \quad 0 < s < 1, \tag{6.24}$$

where u is the transverse displacement of the same material point on the rectangle between the undeformed configuration and the current configuration, $I = \int_{-a}^{a} Y^2 dY = \frac{2}{3}a^3$ is the area moment of inertia, and Λ is the absolute value of the compressive applied force. If we also impose the clamped boundary conditions

$$u(0) = u(1) = 0, \quad u'(0) = u'(1) = 0, \tag{6.25}$$

the smallest positive eigenvalue of (6.24) is $\Lambda = 4\hat{E}I\pi^2$, which is the Euler buckling formula with two clamped ends. By this formula, the first critical stress value (i.e., the smallest absolute critical stress value) is given by $\frac{\Lambda}{2a\hat{E}} = \frac{4}{3}\pi^2 a^2$.

Note that the clamped boundary conditions (6.25) were used in Landau and Lifshitz [25, p. 72], in which the clamped boundary condition was explained as follows: "The end of the rod is said to be clamped if it cannot move either longitudinally or transversely, and moreover its direction (i.e., the direction of the tangent to the rod) cannot change." In section 5, we give the asymptotic clamped boundary conditions (5.10) and (5.11) for a two-dimensional rectangle. There are two significant differences between these two types of clamped boundary conditions. One is that our clamped boundary conditions are related to the axial strain W; see $(5.10)_4$ and $(5.11)_3$. Another is that the tangent values of the axis at two ends are not zeros and are related to constitutive constants and the external forces γ and q; see $(5.10)_2$ and $(5.11)_2$. From the derivations of the asymptotic clamped boundary conditions, we can see that these

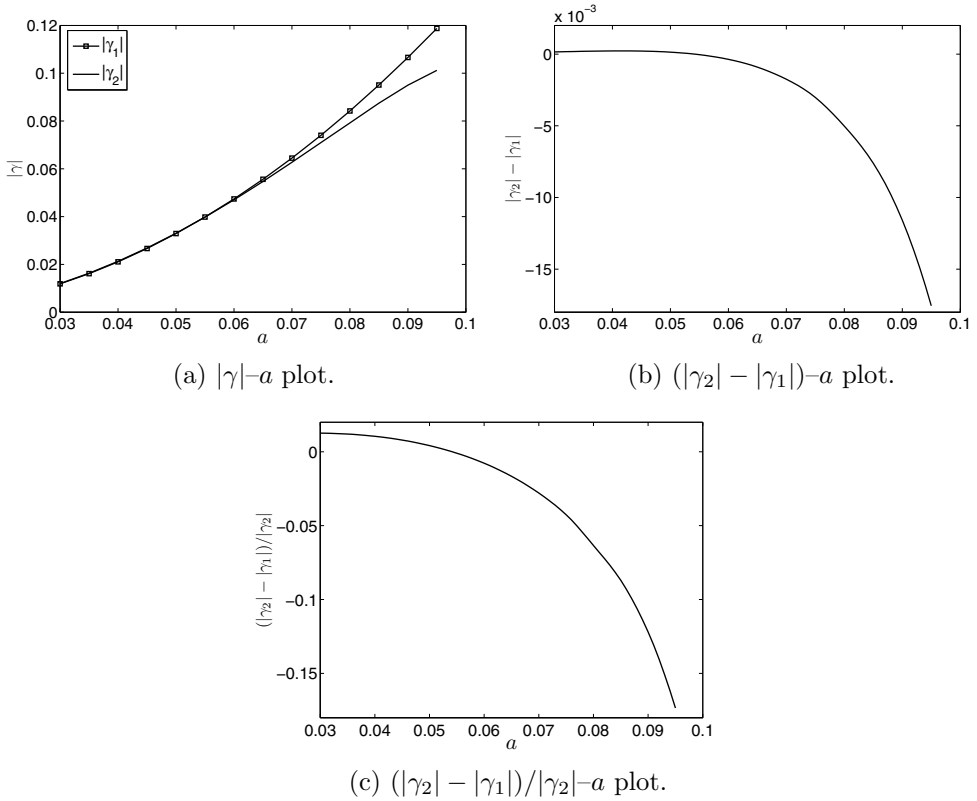

(a) $|\gamma|$–a plot.

(b) $(|\gamma_2| - |\gamma_1|)$–$a$ plot.

(c) $(|\gamma_2| - |\gamma_1|)/|\gamma_2|$–$a$ plot.

FIG. 6.5. *Comparisons of the first critical stress values γ_1 obtained from* (6.24) *with γ_2 obtained from our model equations.*

differences are caused by the geometry of the rectangle, the effects of the nonuniform axial strain, and the nonlinearity of the problem.

In Figure 6.5, we compare the absolute values of the first critical stress values obtained from two different models. In Figure 6.5(a), we give the plots of the first critical stress values $|\gamma_1|$ and $|\gamma_2|$ obtained from (6.24) and our model equations, respectively, as a varies. In Figures 6.5(b) and (c), we give the plots of the difference of the first critical stress value $|\gamma_2| - |\gamma_1|$ and the relative error $(|\gamma_2| - |\gamma_1|)/|\gamma_2|$, respectively.

We find that when $0.03 \le a < 0.0542$, $|\gamma_2| > |\gamma_1|$; when $a > 0.0542$, $|\gamma_2| < |\gamma_1|$. So, according to our results, the Euler buckling formula gives an overestimate of the buckling stress value when the aspect ratio is larger than 0.1084, and an underestimate when it is smaller than 0.1084 (although the error is very small; cf. Figure 6.5). We also observe that when $a < 0.075$, the relative error is smaller than 5%. From the above analysis, we can say that when $0.03 \le a < 0.075$, the Bernoulli–Euler beam equation yields a good result for the buckling stress value, in comparison with that obtained from our model equations.

However, there are some differences between our model equations and the fourth-order linear ODE. Here we study a compressible Murnaghan material. Shearing is taken into account in our derivations. Moreover, our model equations can yield a finite number of bifurcation points only when $0.03 \le a < 0.0955$, while the fourth-order linear ODE can yield an infinite countable number of bifurcation points for slender rectangles.

When $a > 0.075$, the difference between the critical stress values obtained from the Euler buckling formula and our model equations becomes relatively large. Thus, we may conclude that (6.24) is not a good model equation for the uniaxial compression of a rectangle when $a > 0.075$; i.e., we have determined an estimated interval $0.06 < 2a < 0.15$ for the aspect ratio of the rectangle where the Euler buckling formula is valid. In [26], Levinson investigated the plane strain problem of a rectangular parallelepiped composed of an incompressible neo-Hookean material. It was found that his numerical estimate for the buckling load can match the Euler buckling formula when the aspect ratio is smaller than 0.167. In [27], from a three-dimensional elasticity and linear stress strain relationship Kardomateas obtained a characteristic equation to determine the critical load for the buckling of a transversely isotropic rod. For isotropic columns, an improved formula of the Euler load was provided where the thickness effects were taken into account. Numerical computations in that paper showed that when the aspect ratio is smaller than about 0.133, the critical load obtained from that formula converges to the Euler load for a column with one end fixed and the other end free. So, the result here for the upper bound (0.15) of the aspect ratio for the validity of the Euler buckling formula is, to some extent, in agreement with the result of Levinson (0.167) and that of Kardomateas (0.133).

7. Conclusions. For some chosen material constants in a Murnaghan strain energy function, we have found two types of instability phenomena in the compressions of a clamped rectangle: barrelling and buckling. The barrelling instability leads to a corner-like profile on the lateral boundaries of the rectangle. This occurs only when the aspect ratio is relatively large, i.e., when the rectangle is thick enough. More specifically, for the material constants chosen here the lower bound of the aspect ratio for barrelling is 0.376 (cf. the paragraph below Figure 6.3 in section 6.1). Our results also reveal that this corner-like profile is caused by the coupling effect of the material nonlinearity and geometrical size of the rectangle. The analytic solution for the postbifurcation corner-like profile is also obtained. When the rectangle is thin enough, buckling instability occurs instead of barrelling. More specifically, for the material constants chosen here the upper bound of the aspect ratio for buckling is 0.191 (cf. the second paragraph below (6.23)). Numerical computations show that our model equations and the fourth-order linear ODE (6.24) can yield very close first critical stress values when the aspect ratio is less than 0.15. However, when the aspect ratio is larger than 0.15, it appears that the Bernoulli–Euler beam equation cannot model the compression of a rectangle well.

The discovery of a lower bound of the aspect ratio for barrelling and a different upper bound for buckling with clamped ends (which limit the lateral movement) implies that there indeed exists a transition region, which agrees with the experimental results in [8, 9]. The present analytical study appears to shed certain light on this more than 40-year-old mist. We also find that after the barrelling no bifurcation to buckling will happen.

Acknowledgment. The authors would like to thank the referees for helpful suggestions and for pointing out the references [22, 27].

REFERENCES

[1] H. C. Simpson and S. J. Spector, *On barrelling instabilities in finite elasticity*, J. Elasticity, 14 (1984), pp. 103–125.

[2] H. C. Simpson and S. J. Spector, *On barrelling for a special material in finite elasticity*, Quart. Appl. Math., 42 (1984), pp. 99–111.

[3] P. J. Davies, *Buckling and barrelling instabilities in finite elasticity*, J. Elasticity, 21 (1989), pp. 147–192.
[4] P. J. Davies, *Buckling and barrelling instabilities of nonlinearly elastic columns*, Quart. Appl. Math., 49 (1991), pp. 407–426.
[5] A. Goriely, R. Vandiver, and M. Destrade, *Nonlinear Euler buckling*, Proc. R. Soc. Lond. Ser. A Math. Phys. Eng. Sci., 464 (2008), pp. 3003–3019.
[6] H. C. Simpson and S. J. Spector, *On bifurcation in finite elasticity: Buckling of a rectangular rod*, J. Elasticity, 92 (2008), pp. 277–326.
[7] T. J. Healey and E. L. Montes-Pizarro, *Global bifurcation in nonlinear elasticity with an application to barrelling states of cylindrical columns*, J. Elasticity, 71 (2003), pp. 33–58.
[8] M. F. Beatty and D. E. Hook, *Some experiments on the elastic stability of circular rubber bars under end thrust*, Internat. J. Solids Structures, 4 (1968), pp. 623–635.
[9] M. F. Beatty and P. Dadras, *Some experiments on the elastic stability of some highly elastic bodies*, Internat. J. Engrg. Sci., 14 (1976), pp. 233–238.
[10] H.-H. Dai and F.-F. Wang, *Corner instabilities in a slender nonlinearly elastic cylinder: Analytical solutions and formation mechanism*, C. R. Math. Acad. Sci. Paris, 345 (2007), pp. 55–58.
[11] H.-H. Dai and F.-F. Wang, *Bifurcation to a corner-like formation in a slender nonlinearly elastic cylinder: Asymptotic solution and mechanism*, Proc. R. Soc. Lond. Ser. A Math. Phys. Eng. Sci., 464 (2008), pp. 1587–1613.
[12] M. F. Beatty, *A theory of elastic stability for incompressible, hyperelastic bodies*, Internat. J. Solids Structures, 3 (1967), pp. 23–37.
[13] A. H. Willis, *Instability in hollow rubber cylinders subjected to axial loads*, in Proceedings of the Seventh International Congress of Applied Mechanics, London, 1948, Vol. 1, pp. 280–296.
[14] M. F. Beatty, *Topics in finite elasticity*, Appl. Mech. Rev., 40 (1987), pp. 1699–1734.
[15] Y. B. Fu and R. W. Ogden, *Nonlinear stability analysis of pre-stressed elastic bodies*, Contin. Mech. Thermodyn., 11 (1999), pp. 141–172.
[16] H.-H. Dai and Y. Huo, *Asymptotically approximate model equations for nonlinear dispersive waves in incompressible elastic rods*, Acta Mech., 157 (2002), pp. 97–112.
[17] H.-H. Dai and X. J. Fan, *Asymptotically approximate model equations for weakly nonlinear long waves in compressible elastic rods and their comparisons with other simplified model equations*, Math. Mech. Solids, 9 (2004), pp. 61–79.
[18] H.-H. Dai and Z. X. Cai, *Phase transitions in a slender cylinder composed of an incompressible elastic material.* I. *Asymptotic model equation*, Proc. R. Soc. Lond. Ser. A Math. Phys. Eng. Sci., 462 (2006), pp. 75–95.
[19] H.-H. Dai and F.-F. Wang, *Asymptotic Bifurcation Solutions for Compressions of a Clamped Nonlinearly Elastic Rectangle: Transition Region and Barrelling to a Corner-like Profile*, preprint, 2009; available online from http://arxiv.org/abs/0903.3913.
[20] I. S. Gradshteyn and I. M. Ryzhik, *Table of Integrals, Series, and Products*, 2nd ed.: A. Jeffrey, ed., Academic Press, New York, 1980.
[21] H.-H. Dai, D. B. Huang, and Z. R. Liu, *Singular dynamics with application to singular waves in physical problems*, J. Phys. Soc. Japan, 73 (2004), pp. 1151–1155.
[22] A. H. Nayfeh, *Perturbation Methods*, Wiley, New York, 1973.
[23] V. Komkov, *Euler's buckling formula and Wirtinger's inequality*, Internat. J. Math. Ed. Sci. Tech., 14 (1983), pp. 661–668.
[24] S. S. Antman, *Nonlinear Problems of Elasticity*, Springer-Verlag, New York, 1995.
[25] L. D. Landau and E. M. Lifshitz, *Theory of Elasticity*, 3rd ed., translated from J. B. Sykes and W. H. Reid, revised and enlarged by E. M. Lifshitz, A. M. Kosevich, and L. P. Pitaevskii, Pergamon Press, Oxford, 1986.
[26] M. Levinson, *Stability of a compressed neo-Hookean rectangular parallelepiped*, J. Mech. Phys. Solids, 16 (1968), pp. 403–415.
[27] G. A. Kardomateas, *Three-dimensional elasticity solution for the buckling of transversely isotropic rods: The Euler load revisited*, Trans. ASME J. Appl. Mech., 62 (1995), pp. 346–355.